CHEMISTRY
A EUROPEAN JOURNAL

DOI: 10.1002/chem.201300466

Modulating the Optoelectronic Properties of Large, Conjugated, High-Energy Gap, Quaternary Phosphine Oxide Hosts: Impact of the Triplet-Excited-State Location

Zhen Zhang,[a] Zhensong Zhang,[b] Runfeng Chen,[c] Jilin Jia,[a] Chunmiao Han,[a] Chao Zheng,[c] Hui Xu,*[a] Donghui Yu,[a] Yi Zhao,*[b] Pengfei Yan,[a] Shiyong Liu,[b] and Wei Huang*[c]

Abstract: The purposeful modulation of the optoelectronic properties was realised on the basis of a series of the large, conjugated, phosphine oxide hosts 9,9-bis-{4′-[2-(diphenylphosphinoyl)phenoxy]biphenyl-4-yl}-9*H*-fluorene (DDPESPOF), 9,9-bis-{3′-(diphenylphosphinoyl)-4′-[2-(diphenylphosphinoyl)phenoxy]biphenyl-4-yl}-9*H*-fluorene (DDPEPOF), 9-[4′-(9-{4′-[2-(diphenylphosphoryl)phenoxy]biphenyl-4-yl}-9*H*-fluoren-9-yl)biphenyl-4-yl]-9*H*-carbazole (DPESPOFPhCz) and 9-[4′-(9-{3′-(diphenylphosphoryl)-4′-[2-(diphenylphosphoryl)phenoxy]biphenyl-4-yl}-9*H*-fluoren-9-yl)biphenyl-4-yl]-9*H*-carbazole (DPEPOFPhCz). The last two are quaternary with fluorenyls as linking bridges, diphenylphosphine oxide (DPPO) moieties as electron acceptors and diphenylethers and carbazolyls as two different kinds of electron donors. Owing to the fine-organised molecular structures and the mixed indirect and multi-insulating linkages, all of these hosts achieve the same first triplet energy levels (T_1) of 2.86 eV for exothermic energy transfer to phosphorescent dopants. The first singlet energy levels (S_1) and the carrier injection/transportation ability of the hosts were accurately modulated, so that DPESPOFPhCz and DPEPOFPhCz revealed extremely similar optoelectronic properties. However, the T_1 state of the former is localised on fluorenyl, whereas the carbazolyl mainly contributes to the T_1 state of the latter. A lower driving voltages and much higher efficiencies of the devices based on DPESPOFPhCz indicated that the chromophore-localised T_1 state can suppress the quenching effects through realising independent contributions from the different functional groups to the optoelectronic properties and the embedding and protecting effect on the T_1 states by peripheral carrier transporting groups.

Keywords: electrophosphorescence • optoelectronic properties • phosphine oxides • quaternary systems • triplet states

Introduction

Organic semiconductors with optoelectronic performance are developed rapidly in recent years due to their potential applications in information technology and energy fields. For these applications, such as organic light-emitting diodes (OLEDs)[1] and organic solar cells (OSC),[2] both optical and electrical properties of the materials should be optimised to satisfy the specific requirements and sequentially improve the device performance.[3] Owing to abundant organic functional groups and diverse molecular configurations, a great amount of organic molecules is developed to seek the "ideal" organic semiconductor.[4] Nevertheless, because optoelectronic properties are the combined results of various factors,[5] for example, the excited state, the molecular aggregation style and intra- and intermolecular interactions, it is rather complicated and difficult to purposefully construct materials with the preferred performance. Furthermore, the same origin of two or more properties even leads the molecular design in a dilemma, as is the situation of hosts in phosphorescent organic light-emitting diodes (PHOLEDs).[6] One of the main challenges in this field is how to obtain ef-

---

[a] Dr. Z. Zhang, J. Jia, C. Han, Dr. H. Xu, D. Yu, Prof. P. Yan
Key Laboratory of Functional Inorganic Material Chemistry
Ministry of Education
School of Chemistry and Materials
Heilongjiang University
74 Xuefu Road, Harbin 150080 (P.R. China)
Fax: (+86) 451-86608042
E-mail: hxu@hlju.edu.cn

[b] Z. Zhang, Prof. Y. Zhao, Prof. S. Liu
State Key Laboratory on Integrated Optoelectronics
College of Electronics Science and Engineering
Jilin University
2699 Qianjin Street, Changchun 130012 (P.R. China)
E-mail: zhao_yi@jlu.edu.cn

[c] Dr. R. Chen, Dr. C. Zheng, Prof. W. Huang
Key Laboratory for Organic Electronics and
Information Displays (KOLED)
Institute of Advanced Materials (IAM)
Nanjing University of Posts and Telecommunications
Nanjing 210046 (P.R. China)
E-mail: wei-huang@njupt.edu.cn

Supporting information for this article is available on the WWW under http://dx.doi.org/10.1002/chem.201300466.

ficient host materials with both a high first triplet energy levels (T_1) and a good electrical performance, which reflects the intrinsic contradictory between optical and electrical properties, derived from the correlation between excited states and frontier molecular orbitals (FMOs).[7]

Because the first singlet energy level (S_1) is approximately equivalent to the energy gap between the highest occupied molecular orbital (HOMO) and the lowest unoccupied molecular orbital (LUMO), a high S_1 of the hosts, due to high a T_1 required for exothermic energy transfer to phosphors, leads to a big barrier for carrier injection and transportation, which results in a remarkably high driving voltages compared with the fluorescent counterparts.[1g] One of the promising strategies is constructing carrier-transporting-type host materials with high energy gaps, such as phosphine oxide (PO) hosts.[8] To further improve the electrical performance of the hosts, ambipolar hosts with a high T_1 are developed as binary systems through insulating linkages blocking intramolecular interactions between the donor and acceptor moieties.[9] Recently, our groups reported highly efficient PHOLEDs with extremely low driving voltages on the basis of ternary systems composed of a chromophore for a high T_1 and donor and acceptor moieties for improved electrical properties.[10] The linkages between these functional groups were carefully chosen to avoid the interference between the T_1 states and the electrical properties by making these properties contributed by the corresponding moieties.[10a,d] However, although it is facile to tune the location of the HOMO and the LUMO owing to the major contributions of the donor and acceptor moieties to these FMOs, it is still extremely difficult to accurately control the location of the triplet excited states, which is much more serious when further extending the conjugation to quaternary systems.[11] Until now, except for several polymeric hosts with short and insulated repeat units,[12] most of the high energy-gap hosts are small molecules with limited conjugation and functional groups and low molecular weights of less than 1000 $\mathrm{g\,mol^{-1}}$.[9r] Although it is rational that increasing the number of different functional groups in a single molecule can facilitate the more accurate tuning of the optoelectronic properties, the formidable challenge of fixing the triplet-excited-state location still makes the development of efficient quaternary host materials inconclusive. In this sense, the systematical investigation of the relationship between the location of the triplet excited state and the molecular structures of the quaternary host materials is imperative.

In this contribution, we showed the investigation of the modulation of the optoelectronic properties of the quaternary host materials with the strategy of mixed multi-insulating and indirect linkages on the basis of four PO hosts, namely 9,9-bis-{4′-[2-(diphenylphosphinoyl)phenoxy]biphenyl-4-yl}-9*H*-fluorene (DDPESPOF), 9,9-bis-{3′-(diphenylphosphinoyl)-4′-[2-(diphenylphosphinoyl)phenoxy]-biphenyl-4-yl}-9*H*-fluorene (DDPEPOF), 9-[4′-(9-{4′-[2-(diphenylphosphoryl)-phenoxy]biphenyl-4-yl}-9*H*-fluoren-9-yl)biphenyl-4-yl]-9*H*-carbazole (DPESPOFPhCz) and 9-[4′-(9-{3′-(diphenylphosphoryl)-4′-[2-(diphenylphosphoryl)phenoxy]biphenyl-4-yl}-9*H*-fluoren-9-yl)biphenyl-4-yl]-9*H*-carbazole (DPEPOFPhCz) (Figure 1 and Scheme 1), with the building blocks fluorenyl as chromophore for high a T_1, carbazolyl and diphenylether as two different donor moieties and diphenylphosphine oxide (DPPO) as acceptor for improved electrical performance. Owing to the mixed linkage strategy, the T_1s of these compounds are successfully preserved as 2.87 eV for efficient energy transfer to phosphorescent dyes, whereas their S_1s and carrier injection/transportation abilities were readily adjusted by the variation of the number and types of functional groups. It is showed that in these large conjugated systems, fluorenyl, diphenylene and carbazolyl can be involved in triplet excited states. The specific location is sensitive to the substitution positions of functional groups that are different for the DDPEPOF and DPEPOFPhCz. The T_1 states of DDPESPOF and DPESPOFPhCz were absolutely localised on fluorenyls to realise the relatively independent contributions of the functional groups to the optoelectronic properties as expected. As the results, compared with those of DPEPOFPhCz, the full-colour PHOLEDs of DPESPOFPhCz achieved the much better electroluminescent (EL) performance including lower driving voltages, larger luminance and higher efficiencies, even though these two hosts have the extremely similar optoelectronic properties. This investigation establishes a solid example to reveal the significance of controlling the triplet-excited-state location for highly efficient host materials.

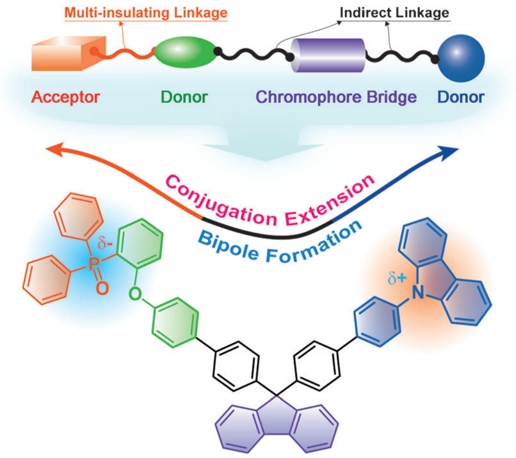

Figure 1. Molecular design of the quaternary PO host DPESPOFPhCz.

Results and Discussion

Design and synthesis: In our previous works of ternary PO hosts, we noticed the location shift of the triplet excited states after conjugation extension and functionalisation, and utilised this phenomenon to realise the convergent tuning of the S_1 and T_1 excited states on the basis of DPEPO-carbazole hybrids.[10d] When further extending the conjugation and incorporating more functional groups, the T_1 excited state localisation of quaternary systems becomes more elu-

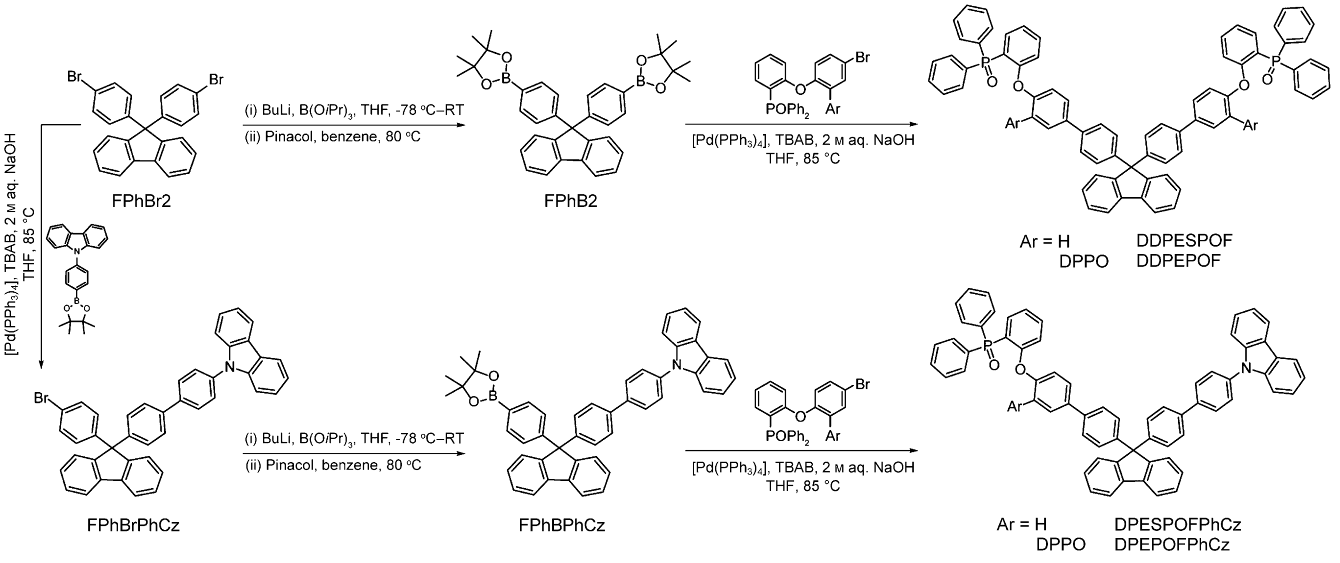

Scheme 1. Synthetic procedure of DDPESPOF, DDPEPOF, DPESPOFPhCz and DPEPOFPhCz. TBAB = tetra-*n*-butylammonium bromide.

sive. However, just because of this, the quaternary system actually provides a good platform for investigating the impact of T_1 excited state location on the electroluminescent performance of the hosts. Nevertheless, the molecular structures of the desired host materials should be carefully designed to achieve high enough T_1 energy levels for efficient energy transfer to dopants and tunable electrical properties for rational comparison.

Considering these pre-requisites, two kinds of effective linkages as indirect and multi-insulating linkages were involved to block the communication between functional groups, facilitating the formation of bipolar structures and preserved T_1s. The indirect linkage was formed through the 9-position of fluorenyl, accompanied with a further conjugation extension through the incorporation of typically multi-insulating DPESPO[10d] or DPEPO.[8] The quaternary systems were further established as the combination of fluorenyl, electron-donating carbazolyl and diphenylether as well as electron-withdrawing DPPO by introducing carbazolyl on the other side of fluorenyl (Figure 1). The asymmetrical configurations of DPESPOFPhCz and DPEPOFPhCz are beneficial to the formation of stable amorphous films.[9q] The other two symmetrical compounds DDPESPOF and DDPEPOF were also prepared with the same considerations (Scheme 1). The high molecular weight of all of these four hosts about 1000 $g\,mol^{-1}$ and their rigid structures might result in an improved thermal and morphological stability.

DDPESPOF, DDPEPOF, DPESPOFPhCz and DPEPOFPhCz were conveniently prepared from the bromide precursor FPhBr2 through forming boric acid and Suzuki coupling with moderate total yields around 40 % (Scheme 1). The structure characterisation was established on the basis of mass spectrometry, NMR spectroscopy and elemental analysis.

DFT simulation: The contributions of different functional groups in quaternary systems to the optoelectronic properties are the focus of this study. The energy levels of the FMOs can provide the referable information for evaluating the carrier-injecting ability. Therefore, density function theory (DFT) calculations on the ground states of DDPESPOF, DDPEPOF, DPESPOFPhCz and DPEPOFPhCz were performed to determine the contributions of the moieties to the FMOs, as well as the formation of bipolar structures. Furthermore, the T_1 states of these molecules were also simulated to obtain the spin-density distributions (SDDs), which indicate the locations of the T_1 excited states (Figure 2).

With the strong electron-donating ability of the O atom in ether, diphenylene formed by one phenylene of diphenylether and another phenylene at the 9-position of fluorenyl make the major contribution to the HOMO of DDPESPOF, whereas its LUMO is mainly localised on the phenyls bonding to P=O by a strong inductive effect accompanied with a minor contribution from fluorenyl. Owing to its extended conjugation, the HOMO energy level of DDPESPOF is remarkably elevated to −5.415 eV compared with its parent molecule DPESPO. Although its LUMO energy level is as high as −0.844 eV, the separated FMOs indicate the ambipolar characteristics of DDPESPOF. Its symmetrical configuration results in the close HOMO and HOMO−1 as well as LUMO and LUMO+1, which is beneficial to the intermolecular charge transfer. Two more DPPOs in DDPEPOF induce the simultaneous decrease of its LUMO and HOMO for 0.163 and 0.326 eV, respectively, ascribed to the same location of the FMOs on fluorenyl and diphenylene. Therefore, the S_1 of DDPEPOF is increased for 0.163 eV, implying its weakened carrier injection ability. After incorporation of carbazolyls in DPESPOFPhCz and DPEPOFPhCz, the HOMO energy levels are dramatically elevated to −5.279 eV owing to the major contribution of the carbazol-

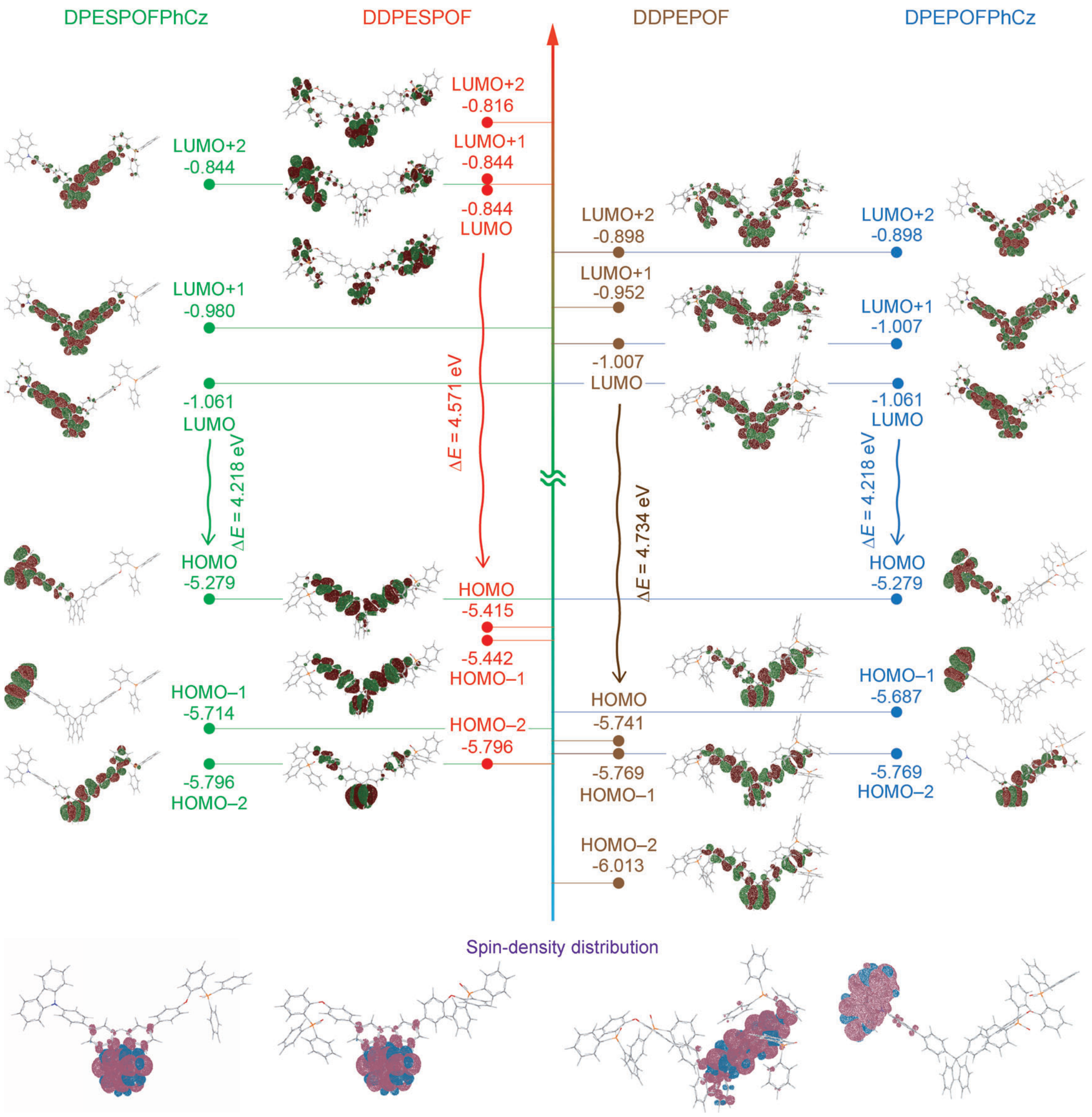

Figure 2. Energy level diagram, molecular configuration and spin-density distribution of the T_1 states of DDPESPOF, DDPEPOF, DPESPOFPhCz and DPEPOFPhCz, simulated by DFT calculations.

yls to the HOMO and HOMO+1. As expected, the incorporation of stronger electron-donating carbazolyl can remarkably improve the hole injection ability. Furthermore, their LUMO energy levels are also changed to −1.061 eV with the decreases of 0.217 and 0.054 eV, respectively, compared with DDPESPOF and DDPEPOF. As the combined result, the S_1s are further reduced for more than 0.35 eV. Noticeably, the indirect and multi-insulating linkages effective suppress the communications between the functional groups, endowing both quaternary DPESPOFPhCz and DPEPOFPhCz with the same FMO energy levels and very similar electron-cloud distributions. It reveals that DDPESPOF, DPESPOFPhCz and DPEPOFPhCz are ambipolar, but DDPEPOF seems to be unipolar.

The T_1 states of these four molecules were also investigated by DFT simulations. Their calculated T_1 energy levels are about 2.90 eV, which further demonstrates the significant effect of the linkage styles on preserving high T_1s. More importantly, according to the contours of the SDDs, the T_1 states of DDPESPOF and DPESPOFPhCz are absolutely contributed by fluorenyl. It was shown that the incorporation of carbazolyl and the variation of the molecular symmetry do not influence the T_1 excited state location. Therefore, the functional groups in DDPESPOF and DPESPOFPhCz as donor, acceptor and chromophore independently contribute to the corresponding optoelectronic properties as expected. However, with additional DPPO bonding to diphenylether, the T_1 state location of DDPEPOF shifts to the diphenylene, whereas carbazolyl in DPEPOFPhCz makes the major contribution to the T_1 state. Obviously, the shift of the T_1 state location is ascribed to the influence of the additional DPPOs, which should be blocked by the combined indirect and multi-insulating linkages as for DDPESPOF and DPESPOFPhCz rather than the single indirect linkage as for DDPEPOF and DPEPOFPhCz. Significantly, DPESPOFPhCz and DPEPOFPhCz exhibited extremely similar properties of FMO distribution and T_1 energy levels, except for their different T_1 state locations, providing a sound platform for investigating the influence of the T_1 state location on the EL performance of the hosts.

Optical properties: The electronic absorption and photoluminescent spectra of DDPESPOF, DDPEPOF, DPESPOFPhCz and DPEPOFPhCz directly show their excited state characteristics (Figure 3 and Table 1). The absorption spectrum of DDPESPOF in dilute solution is composed of three bands around $\lambda = 288$, 261 and 226 nm, which are attributed to an $n\rightarrow\pi^*$ transition from diphenylether to fluorenyl, an $n\rightarrow\pi^*$ transition of diphenylether and a $\pi\rightarrow\pi^*$ transition of DPPO, respectively. For DDPEPOF, the first two bands overlap with the peak at $\lambda = 274$ nm. The incorporation of carbazolyls in DPESPOFPhCz and DPEPOFPhCz results in two new bands around $\lambda = 340$ and 310 nm, corresponding to $n\rightarrow\pi^*$ transitions from carbazolyl to diphenylether and fluorenyl, respectively. The absorption spectra of these four molecules in thin film are similar to those in solution with remained fine structures, which indicates the reduced aggregation in the solid states (Figure SI1 in the Supporting Information). According to the optical energy gaps evaluated by the absorption edges, the S_1 of DDPESPOF is 3.75 eV, and 0.08 eV lower than that of DDPEPOF. The S_1s of DPESPOFPhCz and DPEPOFPhCz are further reduced to 3.51 eV due to absorption extension by the carbazolyl-involved transitions, which is in perfect agreement with the DFT calculation results. The fluorescence (FL) spectra of DDPESPOF, DDPEPOF, DPESPOFPhCz and DPEPOFPhCz in dilute solution are similar. Only a slight bathochromic shift of 17 nm for the emission peaks was observed from DDPESPOF to DPESPOFPhCz. Furthermore, the incorporation of carbazolyl in DPESPOFPhCz and DPEPOFPhCz remarkably reduces the full width at half maximum (FWHM) of their emission from 70 to 50 nm, which implies the suppressed intramolecular interactions. The solid-state emission spectra of DDPESPOF and DDPEPOF are similar with peaks at about $\lambda = 420$ nm (Figure SI1 in the Supporting Information). The bathochromic shifts for DPESPOFPhCz- and DPEPOFPhCz-based films are smaller owing to their asymmetrical configurations for suppressing intermolecular interactions.

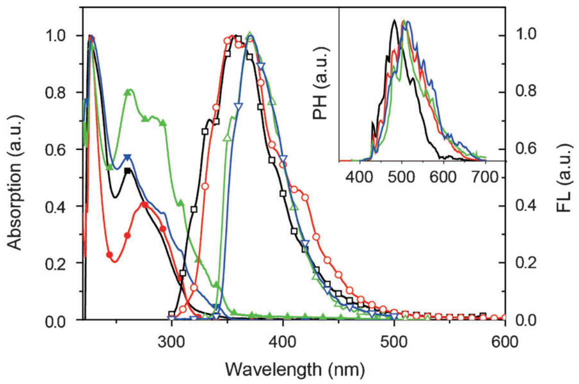

Figure 3. Absorption (solid), fluorescence (FL, hollow) and phosphorescence (PH, inset) spectra of DDPESPOF (black, ■), DDPEPOF (red, ●), DPESPOFPhCz (green, ▲) and DPEPOFPhCz (blue, ▼) in CH_2Cl_2 (10^{-6} mol L^{-1}). The PH spectra were measured at 77 K after a delay of 300 μs.

The suppressed intramolecular interaction of DDPESPOF, DDPEPOF, DPESPOFPhCz and DPEPOFPhCz was further confirmed through their FL spectra in various solvents with different polarity (Figure SI2 in the Supporting Information). The emission of DDPESPOF and DDPEPOF shifts bathochromically along with increasing the solvent polarity with an interval less than 20 nm. It is interesting that with the stronger electron-donating carbazolyls and the ambipolar structures, DPESPOFPhCz and DPEPOFPhCz reveal much more stable emissions with very close emission peaks and similar profiles in different solvents, which might be due to the mixed indirect and insulating linkages that supported effective suppression of intramolecular charge transfer (ICT). Actually, restraining low-energy excited states is the pre-requisite for achieving both ambipolar characteristics and high T_1s.

The time-resolved phosphorescence (PH) spectra of DPESPOF, DDPEPOF, DPESPOFPhCz and DPEPOFPhCz were measured at 77 K to estimate the T_1 energy

Table 1. Physical properties of the PO hosts.

	Absorption [nm]	Emission [nm]	PLQY[c] [%]	S_1 [eV[	T_1 [eV]	$T_g/T_m/T_d$ [°C][h]	RMS [nm]	HOMO [eV]	LUMO [eV]
DDPESPOF	288, 261, 226[a]	319, 330, 357[a]	30.8	3.75[d]	2.87[f]	166/–/531	0.106	–6.20[g]/–5.42[e]	–2.45[g]/–0.84[e]
	298, 262, 230[b]	423[b]		4.57[e]	2.96[e]				
DDPEPOF	274, 227[a]	353, 371[a]	52.9	3.83[d]	2.87[f]	203/–/472	0.162	–6.33[g]/–5.74[e]	–2.50[g]/–1.01[e]
	293, 263, 230[b]	421[b]		4.73[e]	2.96[e]				
DPESPOFPhCz	339, 309, 283, 263, 227[a]	353, 370[a]	25.3	3.51[d]	2.87[f]	238/–/523	0.202	–6.12[g]/–5.28[e]	–2.61[g]/–1.06[e]
	328, 293, 260, 207[b]	370, 403[b]		4.22[e]	2.90[e]				
DPEPOFPhCz	340, 308, 291, 261, 228[a]	353, 371[a]	61.7	3.52[d]	2.87[f]	248/–/475	0.208	–6.12[g]/–5.28[e]	–2.61[g]/–1.06[e]
	326, 289, 259, 226, 205[b]	414[b]		4.22[e]	2.96[e]				

[a] Measured in CH_2Cl_2 (10^{-6} mol L^{-1}). [b] Measured in a film. [c] Calculated by using 9,10-diphenylanthracene as standard. [d] Estimated according to the absorption edges. [e] DFT-calculated results. [f] Calculated according to the 0–0 transitions of the phosphorescence spectra. [g] Calculated according to the equation HOMO/LUMO = 4.78+onset voltage. [h] T_g = temperature of glass transition, T_m = melting point, T_d = temperature of decomposition.

levels according to the 0–0 transitions (inset in Figure 2 and Table 1). The 0–0 transitions of all four compounds are at about $\lambda = 430$ nm, corresponding to a T_1 of 2.87 eV, which is high enough for a positive energy transfer to the commercially available blue phosphor bis(4,6-(difluorophenyl)pyridinato-N,C^2)picolinate iridium(III) (FIrpic, $T_1 = 2.65$ eV). Therefore, we successfully realised the large, conjugated, host materials with rather high T_1s. Their uniform T_1 energy levels should be attributed to the suppression of interference between the functional groups by indirect and multi-insulating linkages, which is in accord with the DFT calculation results.

Obviously, the mixed linkage strategy endows the quaternary DPESPOFPhCz and DPEPOFPhCz with the much reduced S_1 by forming bipolar structures and the preserved T_1 by suppressing intramolecular interplays. As a result, compared with DDPESPOF and DDPEPOF, the energy gaps between S_1 and T_1 are reduced by 0.3 eV. Significantly, as indicated by DFT calculations, DPESPOFPhCz and DPEPOFPhCz exhibit almost the same photophysical properties with the extremely similar spectra from peak wavelengths to profiles, as well as the same excited energy levels.

Carrier injection and transportation properties: Cyclic voltammograms of DDPESPOF, DDPEPOF, DPESPOFPhCz and DPEPOFPhCz were measured to confirm their redox behaviour, which is related to the carrier injection abilities (Figure 4 a). DDPESPOF revealed a semi-reversible oxidation peak with an onset voltage of 1.42 V, corresponding to the oxidation of diphenylene and the HOMO of −6.20 eV (Table 1). Its irreversible reduction peak was observed at −2.84 V with an onset voltage of −2.33 V, corresponding to the LUMO of −2.45 eV. The situation is similar for DDPEPOF, HOMO and LUMO energies of which are −6.33 and −2.50 eV, respectively. DPESPOFPhCz and DPEPOFPhCz also showed an irreversible reduction peak at about −2.6 V with an onset voltage at −2.17 V, corresponding to the LUMO of −2.61 eV. Beside the irreversible oxidation peaks at about 2.1 V, the carbazolyls in DPESPOFPhCz and DPEPOFPhCz give rise to the first semi-reversible oxidation peaks at 1.63 V and result in the HOMO of −6.12 eV. The similar oxidation peaks of DPESPOFPhCz and DPEPOFPhCz further demonstrate the restrained intramolecular interplays between the functional groups. Furthermore, their HOMO–LUMO energy gaps are 3.51 eV, which is exactly equivalent with the results of the optical analysis.

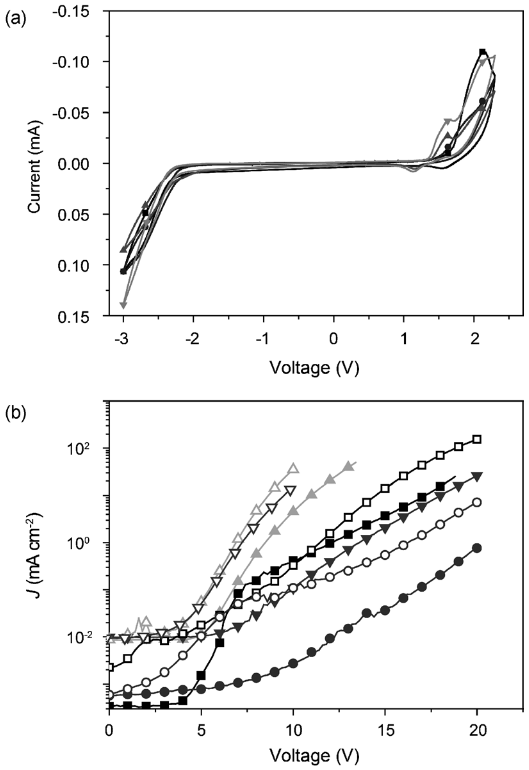

Figure 4. a) Cyclic voltammograms of DPESPOF (■), DDPEPOF (●), DPESPOFPhCz (▲) and DPEPOFPhCz (▼) measured in CH_2Cl_2 with tetra-*n*-butylammonium hexafluorophosphate as supporting electrolyte ($0.1\ mol\,L^{-1}$) at a scanning rate of $100\ mV\,S^{-1}$. b) *IV* characteristics of nominal single-carrier transporting devices based on the hosts (filled symbols = electron-only, open symbols = hole-only).

The nominal single-carrier transporting devices based on DDPESPOF, DDPEPOF, DPESPOFPhCz and DPEPOFPhCz were fabricated to estimate their carrier transporting abilities, whose configurations are ITO|MoO_x (2 nm)|*m*-MTDATA:MoO_x (15 wt %, 30 nm)|*m*-MTDATA (10 nm)|[Ir(ppz)$_3$] (10 nm)|host (30 nm)|[Ir(ppz)$_3$] (10 nm)|*m*-MTDATA (10 nm)|*m*-MTDATA:MoO_x (15 wt %, 30 nm)|MoO_x (2 nm)|Al for hole-only devices and ITO|Cs_2CO_3 (1 nm)|BPhen (40 nm)|host (30 nm)|BPhen (40 nm)|Cs_2CO_3 (1 nm)|Al for electron-only devices, respectively, where MoO_x and Cs_2CO_3 served as hole- and electron-injecting layers, *m*-MTDATA is 4,4′,4′′-tri(*N*-3-methylphenyl-*N*-phenylamino)triphenylamine as the hole-transporting layer (HTL), [Ir(ppz)$_3$] is tris(phenylpyrazole)iridium as the hole-transporting/electron-blocking layer and BPhen is 4,7-diphenyl-1,10-phenanthroline as the electron-transporting hole-blocking layer. The ambipolar characteristic and suitable molecular configuration endow DDPESPOF with the balanced carrier transporting ability indicated by the comparable electron-only and hole-only current densities (*J*; Figure 4 b). The devices based on DDPEPOF showed the smallest hole-only and electron-only *J*, which was mainly originated from its unipolar characteristics. The molecular configuration of DDPEPOF should be another reason why its fluorenyl makes the major contribution to the LUMO, but is embedded by the surrounding moieties. This impeded the intermolecular electron hopping between fluorenyls in adjacent DDPEPOF molecules. It was shown that the hole-transporting carbazolyls in DPESPOFPhCz- and DPEPOFPhCz supported their devices with the strongest hole-transporting ability among these hosts, which was proven by the highest hole-only *J*. The electron-only *J* of DPESPOFPhCz- and DPEPOFPhCz-involved devices was also dramatically improved for several orders of magnitude compared with those of the devices based on DDPESPOF and DDPEPOF, owing to their more rigid and planar structure for efficient intermolecular charge transport.

It was shown that in these large conjugated hosts, the function of the PO groups is mainly focused on enhancing the electron-capture ability of the bonded moieties by a strong inductive effect rather than directly getting involved in carrier transportation. Therefore, the big steric hindrance of the peripheral DPESPO and DPEPO groups in DDPESPOF and DDPEPOF may restrain the intermolecular communication between the electrically active moieties and result in the worse carrier transporting performance. Thus, for large conjugated systems the molecular structure should be one of the determinants for carrier transportation.

Thermal and morphological properties: The investigation of the thermal properties of DDPESPOF, DDPEPOF, DPESPOFPhCz and DPEPOFPhCz was performed by using thermogravimetric analysis (TGA) and differential scanning calorimetry (DSC) (Figure 5 and Table 1). All four hosts exhibited a rather high thermal stability with a temperature of decomposition (T_d) at a weight loss of 5% for more than 450 °C, making the device fabrication by vacuum evaporation feasible. Although the molecular weight of DDPESPOF is 120 g mol^{-1} higher than that of DPESPOFPhCz, their T_d values are almost the same. DDPEPOF and DPEPOFPhCz revealed the similar situation. This is the combined result of the DPPO-induced improvement of the molecular sublimability and the high rigidity of carbazolyl.[8i] For the same reason, the T_d values of DDPEPOF and DPEPOFPhCz are 50 °C lower than those of DDPESPOF and DPESPOFPhCz. DSC analysis showed that no melting point (T_m) was observed during the heating cycles before decomposition of all four hosts (inset in Figure 5 and Table 1), which indicates the facility of forming amorphous states. The temperature of glass transition (T_g) of DDPESPOF is recognised as 166 °C, whereas the high rigidity of carbazolyl in DPESPOFPhCz further improves its T_g for 37 °C. Owing to the steric hindrance of DPPO, the T_g of DDPEPOF is much higher (238 °C). The substitution of the DPEPO moiety with phenylcarbazole in DPEPOFPhCz only results in an increase of 10 °C for T_g. Therefore, both DPPO with high steric hindrance and carbazolyl with high rigidity can contribute to the phase stability. The excellent thermal performance of these large, conjugated, quaternary hosts implies their advantages in device stability by suppressing phase separation during long-term operation.

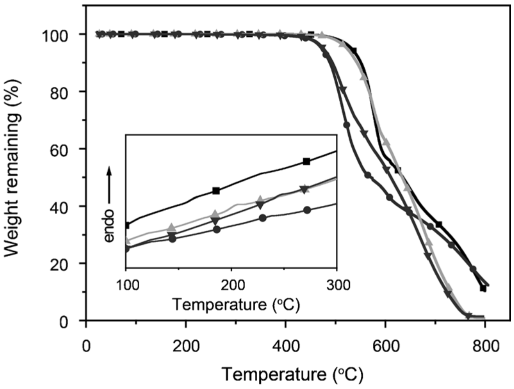

Figure 5. TGA and DSC curves of DDPESPOF (■), DDPEPOF (●), DPESPOFPhCz (▲) and DPEPOFPhCz (▼).

The film formability of these hosts was also investigated with atom force microscopy (AFM) and scanning electronic microscopy (SEM) (Figure 6). The AFM images show that

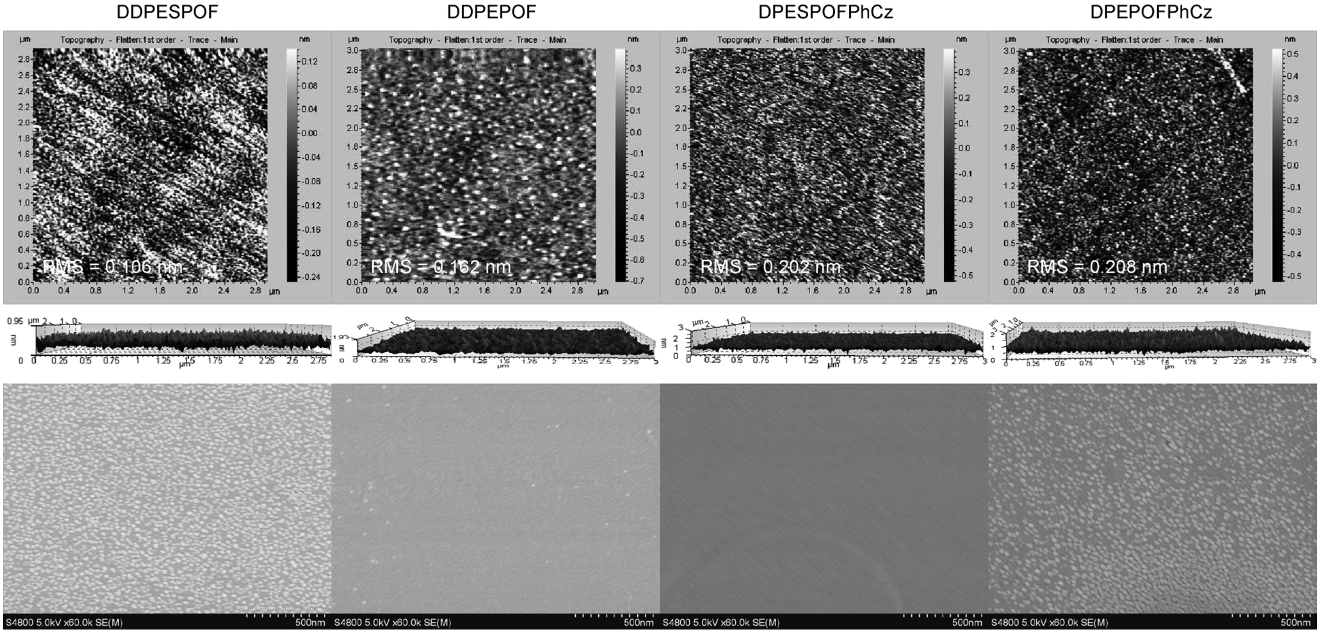

Figure 6. AFM (top) and SEM (bottom) images of vacuum-evaporated thin films of DDPESPOF, DDPEPOF, DPESPOFPhCz and DPEPOFPhCz with a thickness of 100 nm.

through vacuum evaporation all of the hosts can form uniform thin films with regular island-like fine structures in the scale of nanometres, which is beneficial to improve the interfaces with adjacent carrier transporting layers. No crystallisation and aggregation was recognised, which was further verified by SEM images. The film quality was so high that the biggest root mean square roughness (RMS) was only 0.208 nm for a DPEPOFPhCz-based film (Figure 6 and Table 1). The RMS of a DDPESPOF-based film was even as small as 0.106 nm. The films of DDPESPOF and DDPEPOF were smoother than those of their carbazolyl-involved analogues, which might be attributed to the stronger molecular sublimability with more DPPOs and the ordered molecular alignment owing to the symmetrical configuration.

EL performance of blue, green, yellow and red PHOLEDs: The fine-modulated optoelectronic properties of DDPESPOF, DDPEPOF, DPESPOFPhCz and DPEPOFPhCz are the targeted investigation of the specific factors, such as the T_1 excited state location, for feasible EL performance. Therefore, full-colour PHOLEDs based on these hosts were fabricated with the configuration ITO|MoO$_x$ (2 nm)|*m*-MTDATA:MoO$_x$ (15 wt.%, 30 nm)|*m*-MTDATA (10 nm)|[Ir(ppz)$_3$] (10 nm)|host:phosphorescent dopants (y wt%, 10 nm)|BPhen (40 nm)|Cs$_2$CO$_3$ (1 nm)|Al (Scheme 2). FIrpic is involved as blue phosphor ($y=10$) to fabricate the blue PHOLEDs named BA–BD by using DDPESPOF, DDPEPOF, DPESPOFPhCz and DPEPOFPhCz as the host, respectively. Analogously, GA–GD, YA–YD and RA–RD were the green, yellow and red PHOLEDs based on the corresponding phosphors of tris(2-phenylpyridine) iridium(III) ([Ir(ppy)$_3$], $y=6$), iridium(III) bis(4-phenylthieno[3,2-*c*]pyridinato-*N*,*C*^{2}) acetylacetonate (PO-01, $y=6$) and bis(2-methyldibenzo-[f,h]quinoxaline)(acetylacetonate) iridium(III) ([Ir(MDQ)$_2$acac], $y=8$), respectively. The efficient energy transfer from the hosts to the dopants was demonstrated by stable EL spectra of these devices corresponding to the emission of these phosphors during voltage increasing (insets in Figure 7 and Figure SI3 in the Supporting Information). Although the optoelectronic properties of these hosts are different, the peak wavelengths and shapes of the EL emissions were only determined by the dopants rather than the hosts, which revealed the similar location of recombination zones owing to the thin emitting layers (EML) with a thickness of 10 nm.

The current/voltage (*IV*) characteristics of the devices revealed the electrical properties of the EMLs as a combination of hosts and dopants. According to the energy level diagram of the devices, the higher LUMOs and lower HOMOs of the hosts made the contributions of the dopants to the carrier injection/transportation non-ignorable (Scheme 2). DDPESPOF and DPESPOFPhCz endowed their blue PHOLEDs BA and BC with the driving voltages of 2.8 V for onset and <3.8 V at 100 cd m^{-2}, respectively, which were much lower than those of BB and BD that are based on DDPESPOF and DPESPOFPhCz (Figure 7a and Table SI1 in the Supporting Information). The same tendency for *J* was noticed, that is, at the same voltages BA and BC had comparable *J* values, which are bigger than that of BD. And the *J* value of BC was the smallest among these devices. The similar *IV* characteristics of BA and BC might be attributed to the contribution of FIrpic for hole injection and transportation, which made up for the weakness of DDPESPOF in hole injection/transportation ability. This was further proven by the consistency of *J* and the electron-transporting ability of the hosts. The differences between the brightness of BA-BD were much more distinct that DDPESPOF and DPESPOFPhCz endowed their devices BA and BC with the much higher luminance at the same voltages and *J*, compared with BB and BD based on DDPEPOF and DPEPOFPhCz (Figure SI4 in the Supporting Information. Because all of the hosts

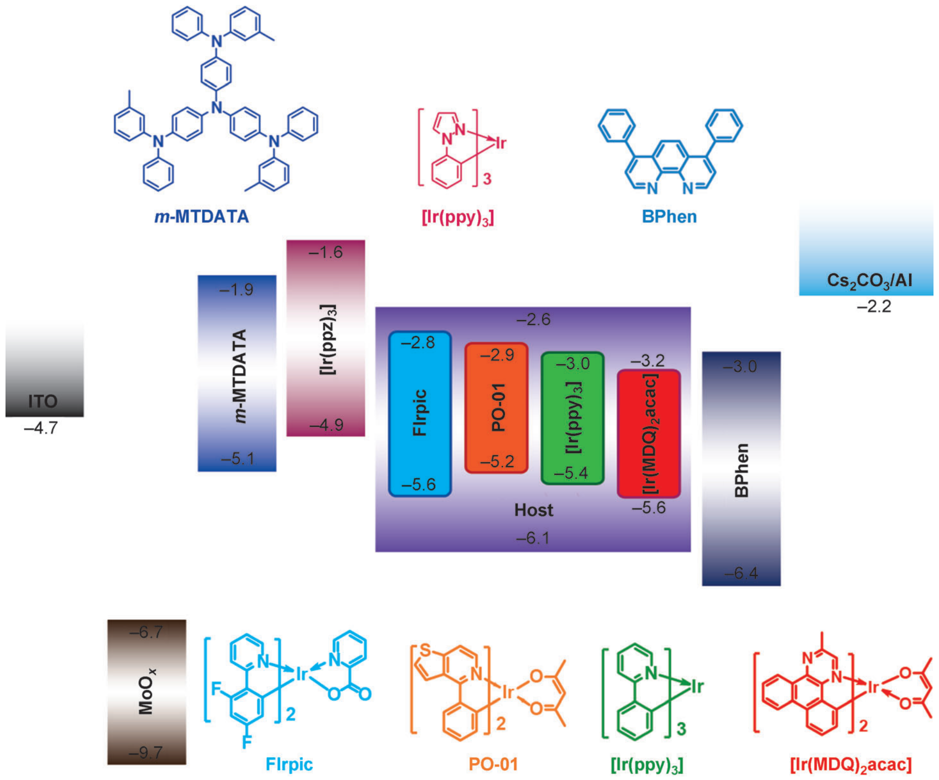

Scheme 2. Device configuration and energy-level diagram of PHOLEDs based on the four different hosts.

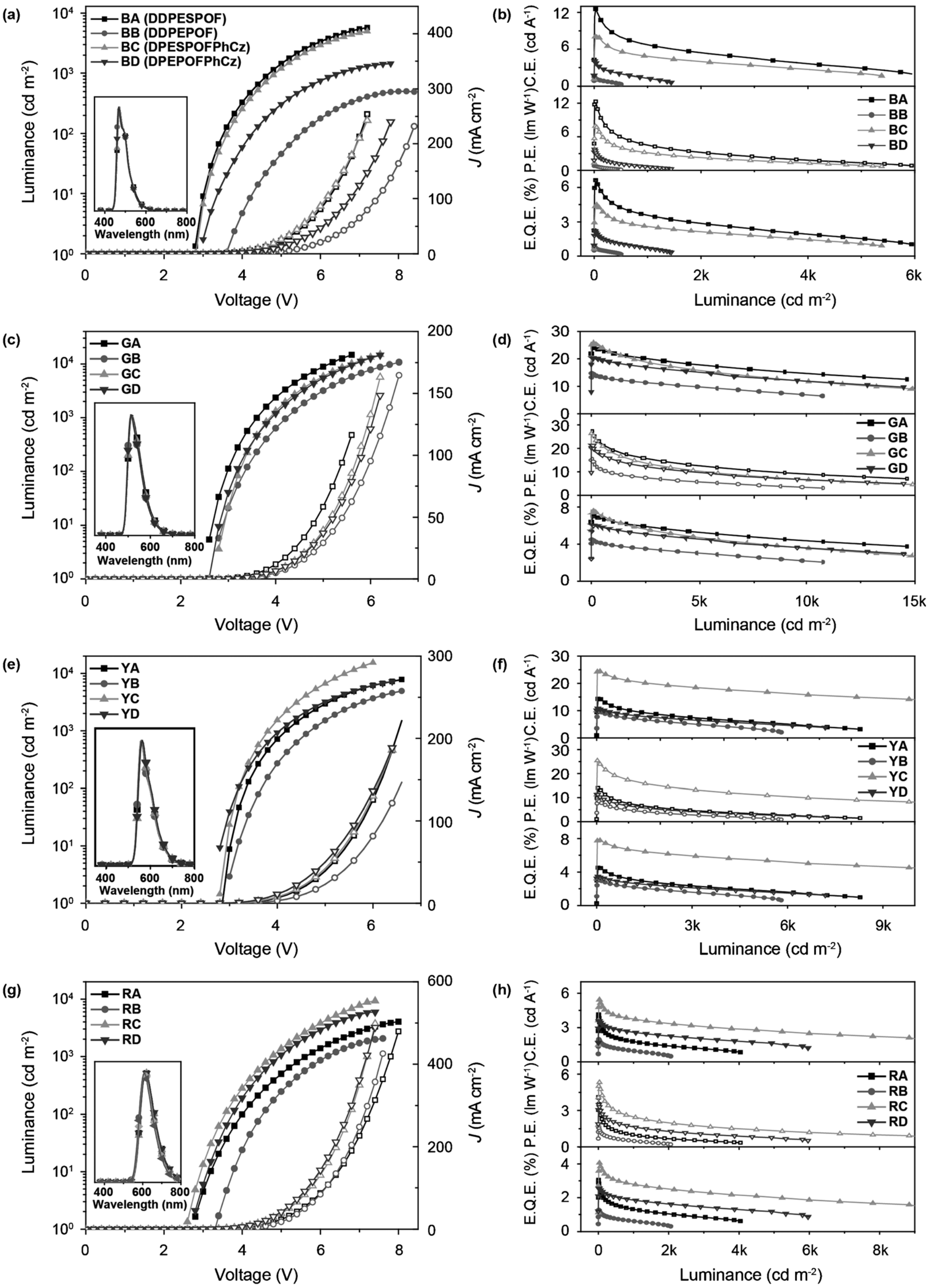

Figure 7. Brightness–current density (J)–voltage (BIV) curves and efficiency–luminance curves of the blue- (a and b), green- (c and d) and red-emitting (e and f) PHOLEDs based on DDPESPOF, DDPEPOF, DPESPOFPhCz and DPEPOFPhCz.

have the same T_1 of 2.86 eV for efficient positive energy transfer to FIrpic, for BA, both of the balance of carrier injection and transportation with the assistance of FIrpic and the stability of the triplet excitons by its fluorene-localised T_1 state should be the main factors for its highest luminance among the devices. The different T_1 state locations in DPESPOFPhCz and DPEPOFPhCz should also be one of the main reasons for the discrepancy between BC and BD in the EL brightness. Suffering from the worst electrical properties and the diphenylene-localised T_1 state of DDPEPOF, its green, yellow and red PHOLEDs, GB, YB and RB, showed the biggest driving voltages and the smallest luminances among the analogous devices. It was shown that the *IV* characteristics of DDPESPOF-based devices were remarkably dependent on the electrical properties of the dopants. Significantly, owing to the stronger electron injection/transportation ability of [Ir(ppy)$_3$], PO-01 and [Ir(MDQ)$_2$acac] with much lower LUMOs around −3.0 eV, the relatively weaker electron transportation in DPEPOFPhCz was reinforced. In this case, the *J* values of its devices GD, YD and RD became comparable with that of the DPESPOFPhCz-based devices GC, YC and RC. Nevertheless, DPESPOFPhCz still supported its devices with a bigger luminance. Especially at high *J*, the brightness of YC and RC can continuously increase, whereas the tendency of the brightness of YD and RD remarkably slowed down, indicating a serious quenching at high exciton concentration. With the same T_1 energy levels and similar *IV* characteristics of their devices, this contrast should be ascribed to the different T_1 state locations of DPESPOFPhCz and DPEPOFPhCz. The simultaneous contribution of carbazolyl to the hole injection/transportation and the T_1 state of DPEPOFPhCz may worsen the polaron–exciton quenching.[13] In this sense, the independent contributions to the optoelectronic properties by different functional groups in the hosts should be superior, especially for the complicated conjugated systems.

It is believed that the high enough T_1 energy levels and the balanced carrier injection/transportation are two main determinants for the efficiency of the host materials. However, the stability of the triplet excitons is also one of the most important factors for device performance. Thus, the impact of the T_1 state location on the EL performance of these hosts was focused in this work, which was further exhibited by the comparison of their device efficiencies. Considering the same T_1 energy levels of these hosts, only the carrier injection/transportation balance and the T_1 state location were involved in the following discussion. The efficiencies of BA were 12.5 cd A^{-1} for the current efficiency (C.E.), 12.3 Lm W^{-1} for the power efficiency (P.E.) and 6.6% for the external quantum efficiency (E.Q.E.), which were the highest values among the blue PHOLEDs (Figure 7b and Table SI1 in the Supporting Information). The DPESPOFPhCz-supported BC had the second high efficiencies of 8.3 cd A^{-1}, 7.9 Lm W^{-1} and 4.5%, which were more than two-folds of those of BB and BD. The much improved EL efficiencies of BA and BC should be the combined result of the relatively balanced carrier transportation and the independent contribution of the fluorenyls to the T_1 states. Owing to the regulation ability of [Ir(ppy)$_3$] with the efficient radiative transition and the good electrical properties, GA, GC and GD achieved high efficiencies of more than 20 cd A^{-1} for the C.E. and 20 Lm W^{-1} for the P.E. Nevertheless, the efficiencies of GC were the highest with 25.9 cd A^{-1}, 26.3 Lm W^{-1} and 7.3%, which were enhanced by 20% compared with those of GD. Because GC and GD exhibited the similar carrier injection and transportation, this improvement should be attributed to the T_1 location of DPESPOFPhCz on its fluorenyl. The situation for the yellow and red PHOLEDs was much different. Because the T_1 energy levels of PO-01 and [Ir(MDQ)$_2$acac] were only 2.2 and 2.0 eV, respectively, the large triplet energy gaps of more than 0.7 eV between the host and the dopant restrain the energy transfer and therefore involve some non-radiative transitions. In this case, the stable T_1 excited state became more important for realising high EL efficiencies. As a result, the efficiencies of YC of 24.4 cd A^{-1}, 25.4 Lm W^{-1} and 7.8% were the highest among the yellow PHOLEDs, which were more than twice of those of YD. Obviously, the much improved efficiencies of YC might originate from the more stable T_1 state of DPESPOFPhCz and the consequential higher host–dopant energy transfer efficiency. The order of the efficiencies of YA–YD actually reflected the contributions of the T_1 excited state location in the hosts and the balanced carrier injection/transportation in the EMLs to the device performance. The DDPESPOF- and DPESPOFPhCz-supported YA and YC had higher efficiencies due to the independent contributions of their functional groups to their optoelectronic properties. The better electrical properties of DPESPOPhCz further resulted in higher efficiencies of YC than those of YA. Although DPEPOPhCz has very similar optoelectronic properties as DPESPOPhCz, its carbazolyl-located T_1 state leaded to much worse efficiencies for YD, which are even lower than those of YA. With the worst electrical properties and the diphenylene-localised T_1 state, it was not surprising that the DDPEPOF-based YB had the lowest efficiencies. Therefore, the location of the T_1 state is at least as equally important as the carrier injection/transportation balance. The situation for RA–RD was similar, as RC achieved the highest efficiencies of 5.4 cd A^{-1}, 5.3 Lm W^{-1} and 4.1%, which were 50% higher than those of RD.

The superiority of DPESPOPhCz can be summarised as follows: 1) Its carrier injection/transportation ability and its T_1 state are contributed by different functional groups, which can suppress the polaron–exciton quenching effect. 2) Its T_1 excited state is localised on fluorenyl, which is embedded and protected from collision-induced quenching by peripheral carrier transporting groups.[13,14] Therefore, DPESPOPhCz can support its devices with a much improved EL performance through blocking several quenching channels. It should also be noticed that the efficiencies of BC with the quaternary DPESPOPhCz were lower than those of its ternary counterparts-based devices, but the efficiencies of their green PHOLEDs were comparable.[10d] This implies that besides of the slightly lower T_1 energy levels, the energy loss induced by structural relaxation originating from the more adjustable groups in the quaternary system, might be one of the main reasons, which had to be considered for the molecular design in subsequent works.

Conclusion

A series of novel large, conjugated, PO hosts, namely DDPESPOF, DDPEPOF, DPESPOFPhCz and DPEPOFPhCz, with high energy gaps was designed and synthesised for the developing of efficient full-colour PHOLEDs.

Through the mixed indirect and multi-insulating linkages, high T_1 energy levels about 2.9 eV were achieved for all of them with a molecular weight about 1000 $g\,mol^{-1}$, which should be a result of suppressed intramolecular interplays between the functional groups. The S_1 energy levels and the electrical properties of these hosts were conveniently and accurately modulated by the variation of the substitution position, the number and the ratio of DPPO, diphenylether and carbazolyl. As a result, two quaternary hosts DPESPOFPhCz and DPEPOFPhCz with very similar optoelectronic properties excluding their different T_1 states contributed by fluorenyl and carbazolyl, respectively, were selected to investigate the impact of the T_1 state location on the EL performance of the hosts. Their full-colour PHOLEDs showed that DPESPOFPhCz endowed its devices with a lower driving voltages and higher efficiencies compared with DPEPOFPhCz. This discrepancy reflects that the independent contribution of the functional groups to the optoelectronic properties is beneficial to restrain the polaron–exciton quenching, and that the embedded T_1 state by peripheral carrier transporting groups can suppress the collision-induced triplet quenching. This work indicated the significance of controlling the T_1 state location for complicated host systems, which may further guide the molecular design of promising multi-functional host materials.

Experimental Section

Materials and instruments: All reagents and solvents used for the synthesis of the compounds were purchased from Aldrich and Acros and used without further purification. 1-(4-Bromophenoxy)-1-[2-(diphenylphosphinoyl)phenoxy]benzene (DPESPOBr),[10d] 4-bromo-2-(diphenylphosphinoyl)-1-[2-(diphenylphosphinoyl)phenoxy]benzene (DPEPOBr),[10d] 9,9-bis(4-bromophenyl)-9*H*-fluorene (FPhBr2)[8n] and 9-{4-[9-(4-bromophenyl)-9*H*-fluoren-9-yl]phenyl}-9*H*-carbazole (FPhCzBr)[10b] were synthesised according to previous reports.

^{1}H NMR spectra were recorded by using a Varian Mercury plus 400NB spectrometer relative to tetramethylsilane (TMS) as internal standard. The molecular mass was determined by a FINNIGAN LCQ by using electro-spraying ionisation-mass spectrometry (ESI-MS) or MALDI-TOF-MS. Elemental analyses were performed on a Vario EL III elemental analyzer. Absorption and photoluminescence (PL) emission spectra of the target compound were measured by using a SHIMADZU UV-3150 spectrophotometer and a SHIMADZU RF-5301PC spectrophotometer, respectively. Thermogravimetric analysis (TGA) and differential scanning calorimetry (DSC) were performed on Shimadzu DSC-60A and DTG-60A thermal analyzers under a nitrogen atmosphere at a heating rate of 10 °C min^{-1}. Cyclic voltammetric (CV) studies were conducted by using an Eco Chemie B.V. AUTOLAB potentiostat in a typical three-electrode cell with a platinum sheet working electrode, a platinum wire counter electrode and a silver/silver nitrate (Ag/Ag^+) reference electrode. All electrochemical experiments were carried out under a nitrogen atmosphere at room temperature in CH_2Cl_2 for oxidation and THF for reduction. Phosphorescence spectra were measured in dichloromethane by using an Edinburgh FPLS 920 fluorescence spectrophotometer at 77 K cooling by liquid nitrogen with a delay of 300 μs by using a time-correlated single photon counting (TCSPC) method with a microsecond-pulsed xenon light source for 10 μs–10 s lifetime measurement, the synchronisation photomultiplier for signal collection and the multi-channel scaling mode of the PCS900 fast counter PC plug-in card for data processing. The thin films of the PO compounds were prepared through vacuum evaporation on glass substrates under the same condition as for device fabrication. The morphological characteristics of these films were measured with an atom force microscope (AFM) Agilent 5100 under the tapping mode and a scanning electron microscope (SEM) HITACHI S-4800 (spraying, accelerating voltage: 5.0 kV, current: 10 mA and observed altitude: 8 mm).

Synthesis

*2,2′-[4,4′-(9*H*-Fluorene-9,9-diyl)bis(4,1-phenylene)]bis(4,4,5,5-tetramethyl-1,3,2-dioxaborolane) (**FPhB2**)*: *n*BuLi (30 mL, 75 mmol) was added into a solution of **FPhBr2** (12 g, 25 mmol) in THF (50 mL) at −78 °C. The mixture was stirred for 1 h at −78 °C, followed by adding triisopropyl borate (35 mL, 150 mmol) dropwise at −78 °C. The solution was allowed to warm to room temperature after 1 h and was stirred for another 24 h at room temperature. A saturated aqueous solution of NH_4Cl (16 g, 300 mmol) was added to the mixture and the resulting solution was stirred for 1 h at 0 °C. The mixture was allowed to warm to room temperature and was then stirred for 12 h. The reaction solution was extracted with diethyl ether (3×50 mL). The combined organic layer was dried with anhydride Na_2SO_4. Benzene (150 mL) and pinacol (17.76 g, 150 mmol) were added after removal the solvent. The reaction solution was extracted by dichloromethane (3×50 mL). The organic layer was dried with anhydrous Na_2SO_4, and then the solvent was removed by distillation in vacuo. The residue was purified by recrystallisation from acetone to afforded the product as white needle crystals (7.1 g, 50 %). ^{1}H NMR (TMS, $CDCl_3$, 400 MHz): $\delta = 7.75$ (d, $J = 7.6$ Hz, 2 H), 7.65 (d, $J = 8.4$ Hz, 4 H), 7.34 (t, $J = 7.2$ Hz, 4 H), 7.23–7.17 (m, 6 H), 1.3 ppm (s, 24 H); LDI-TOF: *m*/*z* (%): 570 [M^+] (100); elemental analysis (%) for $C_{37}H_{40}B_2O_4$: C 77.92, H 7.07, O 11.22; found C 78.01, H 7.08, O 11.34.

*9-(4′-{9-[4-(4,4,5,5-Tetramethyl-1,3,2-dioxaborolan-2-yl)phenyl]-9*H*-fluoren-9-yl}biphenyl-4-yl)-9*H*-carbazole (FPhCzB)*:*n*BuLi (0.6 mL ,1.5 mmol) was added into a solution of FPhCzBr (0.6386 g, 1 mmol) in THF (10 mL) at −78 °C. The mixture was stirred for 1 h at −78 °C, followed by adding triisopropyl borate (0.7 mL, 3 mmol) dropwise at −78 °C. The solution was allowed to warm to room temperature after 1 h and was stirred for another 24 h at RT. A saturated aqueous solution of NH_4Cl (0.321 g, 6 mmol) was added into the mixture and the resulting solution was stirred for 1 h at 0 °C. The mixture was allowed to warm to room temperature and was then stirred for 12 h. The reaction solution was extracted with diethyl ether (3×50 mL). The combined organic layers were dried with anhydrous Na_2SO_4. Benzene (10 mL) and pinacol (0.3545 g, 3 mmol) were added after removal of the solvent. The reaction solution was extracted with dichloromethane (3×50 mL). The dichloromethane extract was dried over anhydrous Na_2SO_4. The solvent was removed in vacuum and the residue was purified by recrystallisation by using acetone. The product was obtained as a white powder (0.41 g, 60 %). ^{1}H NMR (TMS, $CDCl_3$, 400 MHz): $\delta = 8.13$ (d, $J = 7.6$ Hz, 2 H), 7.79 (d, $J = 7.6$ Hz, 2 H), 7.73–7.71 (q, $J_1 = 2.8$, $J_2 = 8.4$ Hz, 4 H), 7.57 (d, $J = 8.4$ Hz, 2 H), 7.50 (d, $J = 8.4$ Hz, 2 H), 7.46–7.35 (m, 8 H), 7.31–7.26 (m, 8 H), 1.31 ppm (s, 12 H); LDI-TOF: *m*/*z* (%): 685 [M^+] (100); elemental analysis (%) for $C_{49}H_{40}BNO_2$: C 85.83, H 5.88, N 2.04, O 4.67; found C 85.78, H 5.91, N 2.11, O 4.72.

*9,9-Bis-{4′-[2-(diphenylphosphinoyl)phenoxy]biphenyl-4-yl}-9*H*-fluorene (DDPESPOF)*: A mixture of FPhB2 (0.5704 g, 1 mmol), DPESPOBr (1.3478 g, 3 mmol), TBAB (0.0323 g, 0.1 mmol), [$Pd(PPh_3)_4$] (0.1156 g, 0.1 mmol) and 2 M NaOH (3 mL,6 mmol) in THF (20 mL) was stirred at 85 °C for 24 h. The organic layer was separated and washed with an ammonium chloride solution. The extract phase was dried with anhydrous Na_2SO_4 and the solvent was removed by distillation in vacuo. The crude product was further purified by flash column chromatography by using methanol/ethyl acetate (1:30) as eluent to give the product as a white powder (0.6 g, 57 %). ^{1}H NMR (TMS, $CDCl_3$, 400 MHz): $\delta = 8.10$–8.05 (dd, $J_1 = J_2 = 7.6$ Hz, 2 H), 7.81–7.75 (m, 10 H), 7.47–7.21(m, 34 H), 6.81–6.78 (dd, $J_1 = 5.2$, $J_2 = 8$ Hz, 2 H), 6.62 ppm (d, $J = 8.8$ Hz, 4 H); LDI-TOF: *m*/*z* (%): 1054 [M^+] (100); elemental analysis (%) for $C_{73}H_{52}O_4P_2$: C 83.10, H 4.97, O 6.07; found C 83.07, H 5.00, O 6.13.

*9,9-Bis-{3′-(diphenylphosphinoyl)-4′-[2-(diphenylphosphinoyl)phenoxy]biphenyl-4-yl}-9*H*-fluorene (DDPEPOF)*: The procedure was similar to that for DDPESPOF except for the use of DPEPOBr (1.9408 g, 3 mmol) instead of DPESPOBr. The desired product was obtained as a white powder (0.8 g, 55 %). ^{1}H NMR (TMS, $CDCl_3$, 400 MHz): $\delta = 7.93$–7.89 (dd, $J_1 = 2$, $J_2 = 13.6$ Hz, 2H), 7.78–7.63 (m, 20H), 7.48–7.14 (m, 42H), 7.08 (t, $J = 7.6$ Hz, 2H), 7.61–7.06 ppm (m, 4H); LDI-TOF: m/z (%): 1454 [M^+] (100); elemental analysis (%) for $C_{97}H_{70}O_6P_4$: C 80.04, H 4.85, O 6.60; found C 80.09, H 4.91, O 6.67.

*9-[4′-(9-{4′-[2-(Diphenylphosphoryl)phenoxy]biphenyl-4-yl}-9*H*-fluoren-9-yl)biphenyl-4-yl]-9*H*-carbazole (DPESPOFPhCz)*: The procedure was similar to that for DDPESPOF except for the use of FPhCzB (0.6857 g, 1 mmol) instead of FPhB2. The residue was purified by column chromatography by using dichloromethane/ethyl acetate (1:2) as eluent to give the product as a white powder (0.23 g, 53 %). ^{1}H NMR (TMS, $CDCl_3$, 400 MHz): $\delta = 8.12$ (d, $J = 8.4$ Hz, 2H), 8.09–8.03 (dd, $J_1 = 7.6$, $J_2 = 12.8$ Hz, 1H), 7.79–7.71 (m, 8H), 7.56 (d, $J = 8.4$ Hz, 2H), 7.52 (d, $J = 8.4$ Hz, 2H), 7.48–7.19 (m, 28H), 6.80–6.76 (dd, $J_1 = 5.2$, $J_2 = 8$ Hz, 1H), 6.61 ppm (d, $J = 8.4$ Hz, 2H); LDI-TOF: m/z (%): 927 [M^+] (100); elemental analysis (%) for $C_{67}H_{46}NO_2P$: C 86.71, H 5.00, N 1.51, O 3.45; found C 86.67, H 5.00, N 1.60, O 3.52.

*9-[4′-(9-{3′-(Diphenylphosphoryl)-4′-[2-(diphenylphosphoryl)phenoxy]biphenyl-4-yl}-9*H*-fluoren-9-yl)biphenyl-4-yl]-9*H*-carbazole (DPEPOFPhCz)*: The procedure was similar to that of DDPEPOF except for the use of FPhCzB (0.6857 g, 1 mmol) instead of FPhB2. The residue was purified by column chromatography by using methanol/ethyl acetate (1:30) as eluent to give the product as a white powder (0.3 g, 53 %). ^{1}H NMR (TMS, $CDCl_3$, 400 MHz): $\delta = 8.14$ (d, $J = 8$ Hz, 2H), 7.95–7.91 (m, 1H), 7.81–7.57 (m, 15H), 7.54–7.24 (m, 33H), 7.15(t, $J = 7.6$ Hz, 1H), 7.07 (t, $J = 7.6$ Hz, 1H), 6.11–6.04 ppm (m, 2H); LDI-TOF: m/z (%): 1127 [M^+] (100); elemental analysis (%) for $C_{79}H_{55}NO_3P_2$: C 84.10, H 4.91, N 1.24, O 4.25; found C 84.14, H 4.89, N 1.32, O 4.33.

DFT calculations: The DFT computations were carried out with different parameters for structure optimisations and vibration analyses. The ground states and triplet states of molecules in vacuum were optimised without any assistance of experimental data by the restricted and unrestricted formalism of Beck's three-parameter hybrid exchange functional[15] and the Lee–Yang–Parr correlation functional[16] (B3LYP)/6-31G(d), respectively. The fully optimised stationary points were further characterised by harmonic vibrational frequency analysis to ensure that real local minima had been found without imaginary vibrational frequency. The total energies were also corrected by the zero-point energy both for the ground state and triplet state. The spin-density distributions were visualised with Gaussview 3.0. All computations were performed using the Gaussian 03 package.[17]

Device fabrication and testing: Prior to the device fabrication, the patterned ITO-coated glass substrates were scrubbed and sonicated consecutively with acetone, ethanol, and de-ionised water, respectively. All the organic layers were thermally deposited in vacuum ($\approx 4.0 \times 10^{-4}$ Pa) at a rate of 1–2 Ås^{-1} monitored in situ with a quartz oscillator. In order to reduce the ohmic loss, a heavily p-doped layer with MoO_x, considering the low doping efficiency in amorphous organic matrix with transition-metal-oxide-based acceptors, was directly deposited onto the ITO substrate for each sample. After the deposition of Cs_2CO_3, the samples were transferred to a metal chamber and suffered from a vacuum break due to the change of the shadow masks to determine the active area. The current–voltage–luminance characteristics were measured with a PR650 spectrascan spectrometer and a Keithley 2400 programmable voltage–current source. All samples were measured directly after fabrication without encapsulation in an ambient atmosphere at room temperature.

Acknowledgements

Z.Z. and Z.S.Z. contributed equally to this work. This work was financially supported by the National Key Basic Research and Development Program of China (2010CB327701), NSFC (50903028, 61176020 and 61275033), the New Century Talents Supporting Program of MOE (NCET-12-0706), Program for Innovative Research Team in University (MOE) (IRT-1237), Key Project of Ministry of Education (212039), a Developing Program of New Century Excellent Talents in Heilongjiang Provincial Universities (1252-NCET-005), the Education Bureau of Heilongjiang Province (10td03) and the Supporting Program of Highlevel Talents of HLJU (2010hdtd08).

---

[1] a) C. W. Tang, S. A. VanSlyke, *Appl. Phys. Lett.* **1987**, *51*, 913; b) J. H. Burroughes, D. D. C. Bradley, A. R. Brown, R. N. Marks, K. Mackay, R. H. Friend, P. L. Burns, A. B. Holmes, *Nature* **1990**, *347*, 539; c) J. Kido, M. Kimura, K. Nagai, *Science* **1995**, *267*, 1332; d) Y. Ma, H. Zhang, J. Shen, C. Che, *Synth. Met.* **1998**, *94*, 245; e) M. A. Baldo, M. E. Thompson, S. R. Forrest, *Nature* **2000**, *403*, 750; f) P. L. Burn, S. C. Lo, I. D. W. Samuel, *Adv. Mater.* **2007**, *19*, 1675; g) S. Reineke, F. Lindner, G. Schwartz, N. Seidler, K. Walzer, B. Lussem, K. Leo, *Nature* **2009**, *459*, 234.

[2] a) G. Yu, J. Gao, J. C. Hummelen, F. Wudl, A. J. Heeger, *Science* **1995**, *270*, 1789; b) U. Bach, D. Lupo, P. Comte, J. E. Moser, F. Weissortel, J. Salbeck, H. Spreitzer, M. Gratzel, *Nature* **1998**, *395*, 583; c) P. Peumans, S. Uchida, S. R. Forrest, *Nature* **2003**, *425*, 158; d) W.-Y. Wong, C.-L. Ho, *Acc. Chem. Res.* **2010**, *43*, 1246; e) L. Dou, W.-H. Chang, J. Gao, C.-C. Chen, J. You, Y. Yang, *Adv. Mater.* **2013**, *25*, 825; f) X. Guo, M. Zhang, J. Tan, S. Zhang, L. Huo, W. Hu, Y. Li, J. Hou, *Adv. Mater.* **2012**, *24*, 6536; g) J. Zhou, X. Wan, Y. Liu, Y. Zuo, Z. Li, G. He, G. Long, W. Ni, C. Li, X. Su, Y. Chen, *J. Am. Chem. Soc.* **2012**, *134*, 16345; h) E. C.-H. Kwok, D. P.-K. Tsang, M.-Y. Chan, V. W.-W. Yam, *Chem. Eur. J.* **2013**, *19*, 2757; i) S. So, K. Lee, P. Schmuki, *Chem. Eur. J.* **2013**, *19*, 2966; j) B. E. Hardin, E. T. Hoke, P. B. Armstrong, J.-H. Yum, P. Comte, T. Torres, J. M. J. Frechet, M. K. Nazeeruddin, M. Gratzel, M. D. McGehee, *Nat. Photonics Nat. Photon.* **2009**, *3*, 406; k) H.-Y. Chen, J. Hou, S. Zhang, Y. Liang, G. Yang, Y. Yang, L. Yu, Y. Wu, G. Li, *Nat. Photonics* **2009**, *3*, 649.

[3] a) X.-H. Zhu, J. Peng, Y. Cao, J. Roncali, *Chem. Soc. Rev.* **2011**, *40*, 3509; b) L.-H. Xie, R. Zhu, Y. Qian, R.-R. Liu, S.-F. Chen, J. Lin, W. Huang, *J. Phys. Chem. Lett.* **2010**, *1*, 272.

[4] W. Huang, B. Mi, Z. Gao, *Organic Electronics*, 1st ed., Science Press, Beijing, **2011**.

[5] M. C. Gather, A. Koehnen, K. Meerholz, *Adv. Mater.* **2011**, *23*, 233.

[6] a) M. A. Baldo, D. F. O'Brien, Y. You, A. Shoustikov, S. Sibley, M. E. Thompson, S. R. Forrest, *Nature* **1998**, *395*, 151; b) C. Adachi, R. C. Kwong, P. Djurovich, V. Adamovich, M. A. Baldo, M. E. Thompson, S. R. Forrest, *Appl. Phys. Lett.* **2001**, *79*, 2082; c) R. J. Holmes, B. W. D'Andrade, S. R. Forrest, X. Ren, J. Li, M. E. Thompson, *Appl. Phys. Lett.* **2003**, *83*, 3818; d) R. J. Holmes, S. R. Forrest, Y.-J. Tung, R. C. Kwong, J. J. Brown, S. Garon, M. E. Thompson, *Appl. Phys. Lett.* **2003**, *82*, 2422.

[7] a) L. Xiao, Z. Chen, B. Qu, J. Luo, S. Kong, Q. Gong, J. Kido, *Adv. Mater.* **2011**, *23*, 926; b) Y. Tao, C. Yang, J. Qin, *Chem. Soc. Rev.* **2011**, *40*, 2943.

[8] a) J.-K. Bin, N.-S. Cho, J.-I. Hong, *Adv. Mater.* **2012**, *24*, 2911; b) M.-k. Leung, W.-H. Yang, C.-N. Chuang, J.-H. Lee, C.-F. Lin, M.-K. Wei, Y.-H. Liu, *Org. Lett.* **2012**, *14*, 4986; c) P. Schrögel, M. Hoping, W. Kowalsky, A. Hunze, G. Wagenblast, C. Lennartz, P. Strohriegl, *Chem. Mater.* **2011**, *23*, 4947; d) J.-H. Jou, W.-B. Wang, S.-Z. Chen, J.-J. Shyue, M.-F. Hsu, C.-W. Lin, S.-M. Shen, C.-J. Wang, C.-P. Liu, C.-T. Chen, M.-F. Wu, S.-W. Liu, *J. Mater. Chem.* **2010**, *20*, 8411; e) H. Fukagawa, N. Yokoyama, S. Irisa, S. Tokito, *Adv. Mater.* **2010**, *22*, 4775; f) D. Hu, P. Lu, C. Wang, H. Liu, H. Wang, Z. Wang, T. Fei, X. Gu, Y. Ma, *J. Mater. Chem.* **2009**, *19*, 6143; g) H.-F. Chen, S.-J. Yang, Z.-H. Tsai, W.-Y. Hung, T.-C. Wang, K.-T. Wong, *J. Mater. Chem.* **2009**, *19*, 8112; h) P. E. Burrows, A. B. Padmaperuma, L. S. Sapochak, P. Djurovich, M. E. Thompson, *Appl. Phys. Lett.* **2006**, *88*, 183503; i) A. B. Padmaperuma, L. S. Sapochak, P. E. Burrows, *Chem. Mater.* **2006**, *18*, 2389; j) P. A. Vecchi, A. B. Padmaperuma, H. Qiao, L. S. Sapochak, P. E. Burrows, *Org. Lett.* **2006**, *8*, 4211; k) H. Xu, G. Xie, C. Han, Z. Zhang, Z. Deng, Y. Zhao, P. Yan, S. Liu, *Org. Electron.* **2012**, *13*, 1516; l) C. Han, Z. Zhang, H. Xu, S. Yue, J. Li, P. Yan, Z. Deng, Y. Zhao, P. Yan, S. Liu, *J. Am. Chem. Soc.* **2012**, *134*, 19179; m) C. Han, G. Xie, H. Xu, Z. Zhang, P. Yan,

Y. Zhao, S. Liu, *Dyes Pigm.* **2012**, *94*, 561; n) D. Yu, Y. Zhao, H. Xu, C. Han, D. Ma, Z. Deng, S. Gao, P. Yan, *Chem. Eur. J.* **2011**, *17*, 2592; o) C. Han, Y. Zhao, H. Xu, J. Chen, Z. Deng, D. Ma, Q. Li, P. Yan, *Chem. Eur. J.* **2011**, *17*, 5800; p) C. Han, G. Xie, H. Xu, Z. Zhang, D. Yu, Y. Zhao, P. Yan, Z. Deng, S. Liu, *Chem. Eur. J.* **2011**, *17*, 445; q) C. Han, G. Xie, H. Xu, Z. Zhang, L. Xie, Y. Zhao, S. Liu, W. Huang, *Adv. Mater.* **2011**, *23*, 2491; r) C. Han, G. Xie, J. Li, Z. Zhang, H. Xu, Z. Deng, Y. Zhao, P. Yan, S. Liu, *Chem. Eur. J.* **2011**, *17*, 8947; s) J. Li, T. Zhang, Y. Liang, R. Yang, *Adv. Funct. Mater.* **2013**, *23*, 619; t) F. May, M. Al-Helwi, B. Baumeier, W. Kowalsky, E. Fuchs, C. Lennartz, D. Andrienko, *J. Am. Chem. Soc.* **2012**, *134*, 13818; u) B. Zhang, G. Tan, C.-S. Lam, B. Yao, C.-L. Ho, L. Liu, Z. Xie, W.-Y. Wong, J. Ding, L. Wang, *Adv. Mater.* **2012**, *24*, 1873.

[9] a) S. Ye, Y. Liu, J. Chen, K. Lu, W. Wu, C. Du, Y. Liu, T. Wu, Z. Shuai, G. Yu, *Adv. Mater.* **2010**, *22*, 4167; b) R.-F. Chen, G.-H. Xie, Y. Zhao, S.-L. Zhang, J. Yin, S.-Y. Liu, W. Huang, *Org. Electron.* **2011**, *12*, 1619; c) Y.-M. Chen, W.-Y. Hung, H.-W. You, A. Chaskar, H.-C. Ting, H.-F. Chen, K.-T. Wong, Y.-H. Liu, *J. Mater. Chem.* **2011**, *21*, 14971; d) S. Gong, Q. Fu, Q. Wang, C. Yang, C. Zhong, J. Qin, D. Ma, *Adv. Mater.* **2011**, *23*, 4956; e) S. Gong, Y. Chen, C. Yang, C. Zhong, J. Qin, D. Ma, *Adv. Mater.* **2010**, *22*, 5370; f) W.-S. Han, H.-J. Son, K.-R. Wee, K.-T. Min, S. Kwon, I.-H. Suh, S.-H. Choi, D. H. Jung, S. O. Kang, *J. Phys. Chem. C* **2009**, *113*, 19686; g) J. He, H. Liu, Y. Dai, X. Ou, J. Wang, S. Tao, X. Zhang, P. Wang, D. Ma, *J. Phys. Chem. C* **2009**, *113*, 6761; h) Z. Ge, T. Hayakawa, S. Ando, M. Ueda, T. Akiike, H. Miyamoto, T. Kajita, M.-a. Kakimoto, *Org. Lett.* **2008**, *10*, 421; i) K. S. Son, M. Yahiro, T. Imai, H. Yoshizaki, C. Adachi, *Chem. Mater.* **2008**, *20*, 4439; j) S. J. Su, H. Sasabe, T. Takeda, J. Kido, *Chem. Mater.* **2008**, *20*, 1691; k) D. Kim, V. Coropceanu, J.-L. Brédas, *J. Am. Chem. Soc.* **2011**, *133*, 17895; l) S. J. Su, C. Cai, J. Kido, *Chem. Mater.* **2011**, *23*, 274; m) H. Huang, Y. Wang, B. Pan, X. Yang, L. Wang, J. Chen, D. Ma, C. Yang, *Chem. Eur. J.* **2013**, *19*, 1828; n) Z. M. Hudson, Z. Wang, M. G. Helander, Z.-H. Lu, S. Wang, *Adv. Mater.* **2012**, *24*, 2922; o) M.-S. Lin, L.-C. Chi, H.-W. Chang, Y.-H. Huang, K.-C. Tien, C.-C. Chen, C.-H. Chang, C.-C. Wu, A. Chaskar, S.-H. Chou, H.-C. Ting, K.-T. Wong, Y.-H. Liu, Y. Chi, *J. Mater. Chem.* **2012**, *22*, 870; p) J. Ye, C.-J. Zheng, X.-M. Ou, X.-H. Zhang, M.-K. Fung, C.-S. Lee, *Adv. Mater.* **2012**, *24*, 3410; q) E. Mondal, W.-Y. Hung, H.-C. Dai, K.-T. Wong, *Adv. Funct. Mater.* **2013**, DOI: 10.1002/adfm.201202889; r) K. S. Yook, J. Y. Lee, *Adv. Mater.* **2012**, *24*, 3169; s) L. Sapochak, A. B. Padmaperuma, P. A. Vecchi, X. Cai, P. E. Burrows, *Proc. SPIE-Int. Soc. Opt. Eng.* **2007**, *6655*, 665506; t) X. Cai, A. B. Padmaperuma, L. S. Sapochak, P. A. Vecchi, P. E. Burrows, *Appl. Phys. Lett.* **2008**, *92*, 083308; u) F.-M. Hsu, C.-H. Chien, C.-F. Shu, C.-H. Lai, C.-C. Hsieh, K.-W. Wang, P.-T. Chou, *Adv. Funct. Mater.* **2009**, *19*, 2834; v) S. O. Jeon, K. S. Yook, C. W. Joo, J. Y. Lee, *Adv. Funct. Mater.* **2009**, *19*, 3644; w) A. Padmaperuma, *Proc. SPIE-Int. Soc. Opt. Eng.* **2009**, *7415*, 74150H; x) E. Polikarpov, J. S. Swensen, N. Chopra, F. So, A. B. Padmaperuma, *Appl. Phys. Lett.* **2009**, *94*, 223304; y) H.-H. Chou, C.-H. Cheng, *Adv. Mater.* **2010**, *22*, 2468; z) S. O. Jeon, K. S. Yook, C. W. Joo, J. Y. Lee, *Adv. Mater.* **2010**, *22*, 1872; aa) D. Kim, S. Salman, V. Coropceanu, E. Salomon, A. B. Padmaperuma, L. S. Sapochak, A. Kahn, J.-L. Bredas, *Chem. Mater.* **2010**, *22*, 247; ab) Y. J. Cho, J. Y. Lee, *Chem. Eur. J.* **2011**, *17*, 11415; ac) S. O. Jeon, S. E. Jang, H. S. Son, J. Y. Lee, *Adv. Mater.* **2011**, *23*, 1436; ad) X. Yang, H. Huang, B. Pan, M. P. Aldred, S. Zhuang, L. Wang, J. Chen, D. Ma, *J. Phys. Chem. C* **2012**, *116*, 15041; ae) H. Sasabe, N. Toyota, H. Nakanishi, T. Ishizaka, Y.-J. Pu, J. Kido, *Adv. Mater.* **2012**, *24*, 3212.

[10] a) C. Han, Z. Zhang, H. Xu, J. Li, G. Xie, R. Chen, Y. Zhao, W. Huang, *Angew. Chem.* **2012**, *124*, 10251; *Angew. Chem. Int. Ed.* **2012**, *51*, 10104; b) D. Yu, F. Zhao, C. Han, H. Xu, J. Li, Z. Zhang, Z. Deng, D. Ma, P. Yan, *Adv. Mater.* **2012**, *24*, 509; c) C. Han, Z. Zhang, H. Xu, J. Li, Y. Zhao, P. Yan, S. Liu, *Chem. Eur. J.* **2013**, *19*, 1385; d) C. Han, Z. Zhang, H. Xu, G. Xie, J. Li, Y. Zhao, Z. Deng, S. Liu, P. Yan, *Chem. Eur. J.* **2013**, *19*, 141.

[11] D. Chaudhuri, H. Wettach, S. K. J. van, S. Liu, E. Sigmund, S. Hoeger, J. M. Lupton, *Angew. Chem.* **2010**, *122*, 7880; *Angew. Chem. Int. Ed.* **2010**, *49*, 7714.

[12] a) Y. Kawamura, S. Yanagida, S. R. Forrest, *J. Appl. Phys.* **2002**, *92*, 87; b) S. Shao, J. Ding, T. Ye, Z. Xie, L. Wang, X. Jing, F. Wang, *Adv. Mater.* **2011**, *23*, 3570.

[13] J. Kalinowski, W. Stampor, J. Mecedilzdotyk, M. Cocchi, D. Virgili, V. Fattori, P. Di Marco, *Phys. Rev. B* **2002**, *66*, 235321.

[14] a) M. A. Baldo, C. Adachi, S. R. Forrest, *Phys. Rev. B* **2000**, *62*, 10967; b) N. C. Giebink, S. R. Forrest, *Phys. Rev. B* **2008**, *77*, 235215; c) S. Reineke, K. Walzer, K. Leo, *Phys. Rev. B* **2007**, *75*, 125328.

[15] A. D. Becke, *J. Chem. Phys.* **1993**, *98*, 5648.

[16] C. Lee, W. Yang, R. G. Parr, *Phys. Rev. B* **1988**, *37*, 785.

[17] Gaussian 03, Revision D.02, M. J. Frisch, G. W. Trucks, H. B. Schlegel, G. E. Scuseria, M. A. Robb, J. R. Cheeseman, J. A. Montgomery, Jr., T. Vreven, K. N. Kudin, J. C. Burant, J. M. Millam, S. S. Iyengar, J. Tomasi, V. Barone, B. Mennucci, M. Cossi, G. Scalmani, N. Rega, G. A. Petersson, H. Nakatsuji, M. Hada, M. Ehara, K. Toyota, R. Fukuda, J. Hasegawa, M. Ishida, T. Nakajima, Y. Honda, O. Kitao, H. Nakai, M. Klene, X. Li, J. E. Knox, H. P. Hratchian, J. B. Cross, V. Bakken, C. Adamo, J. Jaramillo, R. Gomperts, R. E. Stratmann, O. Yazyev, A. J. Austin, R. Cammi, C. Pomelli, J. W. Ochterski, P. Y. Ayala, K. Morokuma, G. A. Voth, P. Salvador, J. J. Dannenberg, V. G. Zakrzewski, S. Dapprich, A. D. Daniels, M. C. Strain, O. Farkas, D. K. Malick, A. D. Rabuck, K. Raghavachari, J. B. Foresman, J. V. Ortiz, Q. Cui, A. G. Baboul, S. Clifford, J. Cioslowski, B. B. Stefanov, G. Liu, A. Liashenko, P. Piskorz, I. Komaromi, R. L. Martin, D. J. Fox, T. Keith, M. A. Al-Laham, C. Y. Peng, A. Nanayakkara, M. Challacombe, P. M. W. Gill, B. Johnson, W. Chen, M. W. Wong, C. Gonzalez, J. A. Pople, Gaussian, Inc., Wallingford CT, **2004**.

Received: February 5, 2013
Revised: March 27, 2013

Optoelectronic Properties

Z. Zhang, Z. Zhang, R. Chen, J. Jia, C. Han, C. Zheng, H. Xu, D. Yu, Y. Zhao,* P. Yan, S. Liu, W. Huang** .... ■■■■–■■■■

Modulating the Optoelectronic Properties of Large, Conjugated, High-Energy Gap, Quaternary Phosphine Oxide Hosts: Impact of the Triplet-Excited-State Location

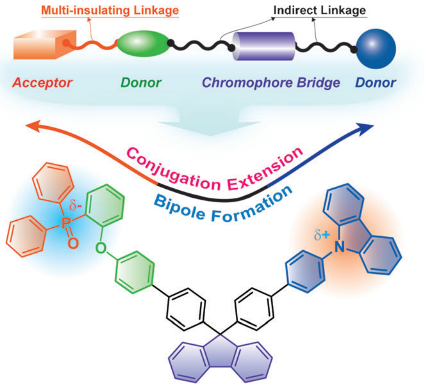

Electrophosphorescence: The modulation of the optoelectronic properties for a series of large, conjugated, quaternary phosphine oxide hosts was realised by the mixed indirect and multi-insulating linkages (see figure). The impact of the triplet state location of the hosts on the electrophosphorescent performance was investigated. A host with a fluorenyl-localised triplet state realised a lower driving voltages and higher efficiencies.